scientific reports

Check for updates

OPEN

Proteomic analysis of CD29+ Müller cells reveals metabolic reprogramming in rabbit myopia model

Chae-Eun Moon[1,5], Jun-Ki Lee[1,5], Hyunjin Kim[1], Ji-Min Kwon[1], Yujin Kang[1,2], Jinu Han[3], Yong Woo Ji[4,5✉] & Yuri Seo[4,5✉]

The prevalence of myopia is rapidly increasing, significantly impacting the quality of life of affected individuals. Prior research by our group revealed reactive gliosis in Müller cells within myopic retina, prompting further investigation of their role in myopia, which remains unclear. In this study, we analyzed protein expression changes in CD29+ Müller cells isolated from a form deprivation-induced rabbit model of myopia using magnetic activated cell sorting to investigate the role of these cells in myopia. As the principal glial cells in the retina, Müller cells exhibited significant alterations in the components of metabolic pathways, particularly glycolysis and angiogenesis, including the upregulation of glycolytic enzymes, such as lactate dehydrogenase A and pyruvate kinase, implicated in the adaptation to increased metabolic demands under myopic stress. Additionally, a decrease in the expression of proteins associated with oxygen transport suggested enhanced vulnerability to oxidative stress. These findings highlight the proactive role of CD29+ Müller cells in modifying the retinal environment in response to myopic stress and provide valuable insights into mechanisms that could help mitigate myopia progression.

Keywords Myopia, Müller cells, Proteomics, Oxidative stress, Glycolysis

Myopia, commonly known as nearsightedness, is a prevalent vision condition wherein objects at a distance appear blurred owing to axial elongation of the eyeball. The prevalence of myopia is increasing, and 4.758 billion people are expected to have myopia by 2050 (48.8% of the global population)[1]. The progression of myopia results in visual impairment due to functional deterioration, thus affecting various aspects of the quality of life of patients[2]. In addition, the financial burden of myopia on families includes both the cost of optical devices and long-term disease management by ophthalmologists[3].

Despite extensive research, critical gaps remain in our understanding of the precise mechanisms underlying the onset and progression of myopia. Recent studies suggest that oxidative stress, not only in the sclera but also within the retinal environment, plays a crucial role in the development of myopia[4–6]. Our prior proteomic analyses have identified proteins linked to oxidative stress and inflammatory reactions within the retina of a rabbit model of myopia[7]. However, the specific contributions of Müller cells – the principal glial cells of the retina– remain inadequately explored[8]. These cells extend radially across the entire thickness of the retina and are involved in various functions, including ion regulation, neurotransmitter recycling, and water transport[8]. In addition, these cells are known to undergo reactive gliosis, a process marked by cellular hypertrophy and proliferation, in response to stress conditions such as diabetic retinopathy, glaucoma, and retinal detachment[9–12]. Additionally, reactive gliosis of Müller cells has been observed in myopia-induced retina in our previous study.

Given the critical roles of Müller cells in maintaining retinal integrity and responding to stress, this study explores their potential contributions to the pathophysiology of myopia, aiming to enrich our understanding

[1]Department of Ophthalmology, Institute of Vision Research, Severance Hospital, Yonsei University College of Medicine, 50 Yonsei-ro, Seodaemun-gu, Seoul 03722, Republic of Korea. [2]Department of Chemical and Biomolecular Engineering, Yonsei University, 50 Yonsei-ro, Seodaemun-gu, Seoul 03722, Republic of Korea. [3]Department of Ophthalmology, Gangnam Severance Hospital, Yonsei University College of Medicine, 211, Eounju-ro, Gangnam-gu, Seoul 03722, Republic of Korea. [4]Department of Ophthalmology, Yongin Severance Hospital, Yonsei University College of Medicine, Yongin-si 16995, Gyeonggi-do, Republic of Korea. [5]Chae-Eun Moon and Jun-Ki Lee contributed equally to this work as the first authors. Yong Woo Ji and Yuri Seo contributed equally to this work as the corresponding authors. ✉email: lusita30@yuhs.ac; yrseo@yuhs.ac

of their involvement. We hypothesized that Müller cells play a central role in the development of myopia and aimed to examine the myopia-associated changes in the Müller cell proteome. To investigate this hypothesis, we isolated Müller cells from the retina of myopia-induced rabbits and conducted a proteomic analysis to identify the molecular changes associated with myopia (Fig. 1). The primary aim of this study was to examine myopia-associated changes in the Müller cell proteome in order to understand the molecular pathophysiology and identify potential targets for therapeutic intervention in myopia.

Results

Myopic changes in rabbit eyes subjected to form deprivation

The myopia group exhibited significant changes in the refractive error when compared to the control group (-2.17 ± 0.76 D vs. -0.83 ± 0.29 D, respectively) (Fig. 2a). Furthermore, axial length measurements showed substantial elongation in the former (2.27 ± 0.8 mm vs. 1.19 ± 0.59 mm, respectively) (Fig. 2b). Additionally, H&E staining results confirmed that no inflammation was present in either group, indicating that the form deprivation and eyelid suturing did not induce adverse inflammatory responses. Consistent with previous findings, significant scleral thinning was observed in the myopic eyes, particularly in the posterior sclera, further validating the successful induction of myopia in this rabbit model (Supplementary Fig. S1).

Confirmation of reactive gliosis in Müller cells during myopia

Following our initial observations that reactive gliosis occurred in Müller cells after myopia induction in rabbit eyes, further examination was conducted to assess whether these changes persisted. Glial fibrillary acidic protein (GFAP) immunostaining was performed on retinal tissues from myopic rabbits. Our results confirmed the
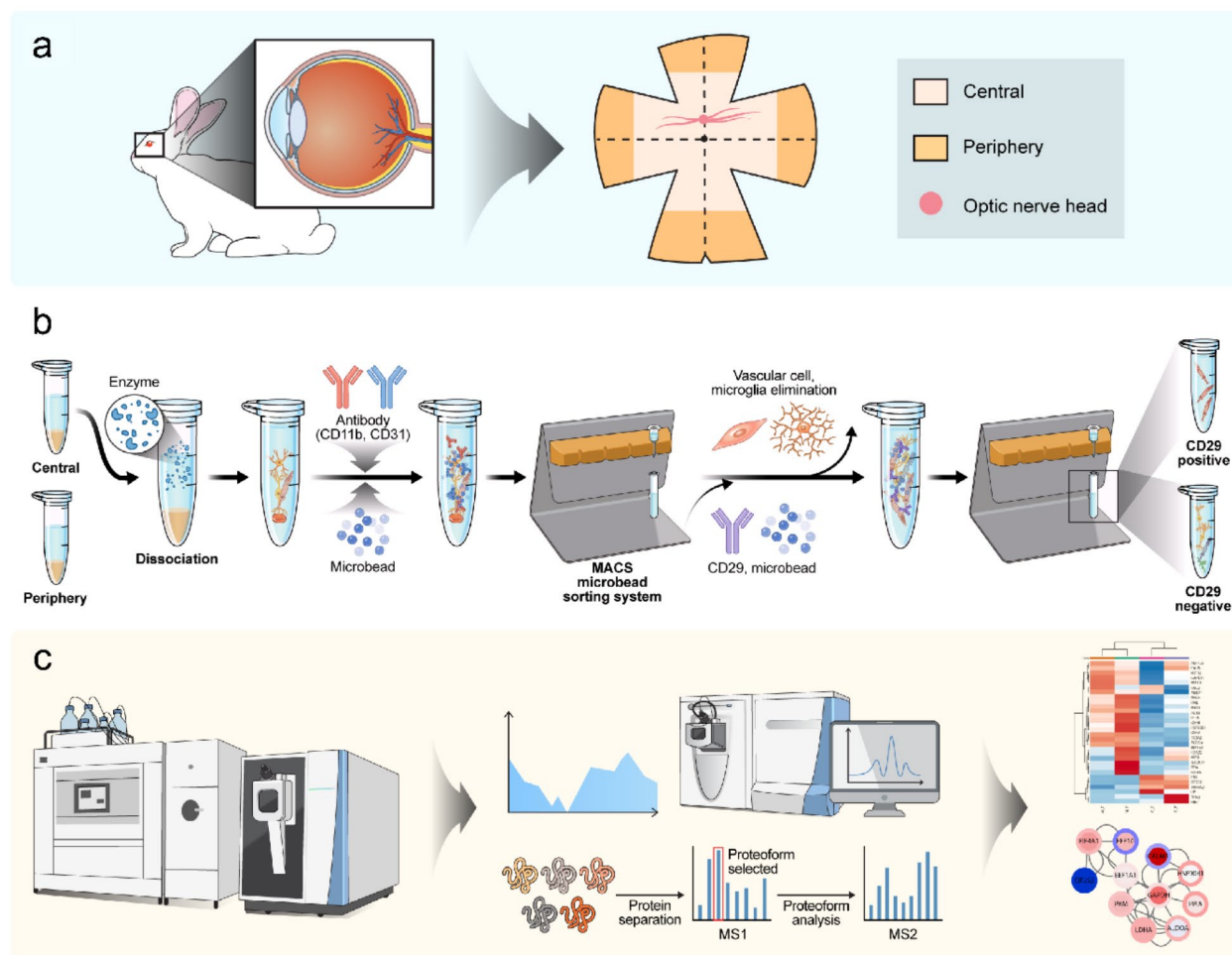

Fig. 1. Representation of proteomic analysis of Müller cells derived from the retina of myopia-induced rabbits. (**a**) Establishment of a myopia model in rabbits through form deprivation. The retina was segmented into central and peripheral regions based on the distance from the visual streak to the limbus. The central retina was defined as the area within 4 mm from the visual streak, while the peripheral retina included areas beyond this boundary. (**b**) Isolation of Müller cells from both the central and peripheral regions of the retina using magnetic-activated cell sorting (MACS) with CD29 antibody selection. (**c**) Subsequent proteomic analysis performed on the isolated Müller cells.
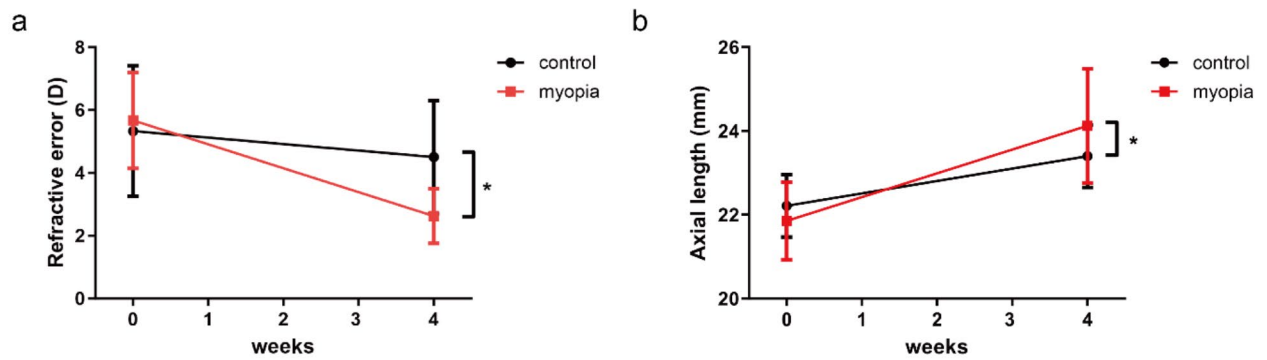
Fig. 2. Change in the refractive error and axial length after form deprivation myopia induction. Compared to the control eye, the myopic eye showed significant reduction in the refractive error and axial elongation.
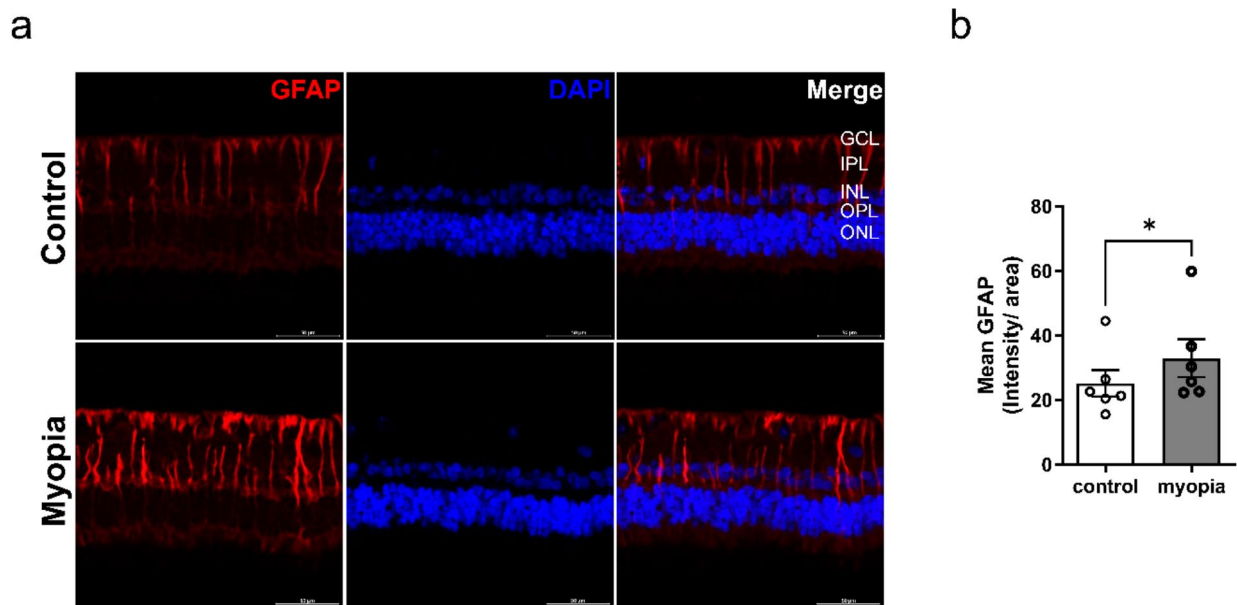

Fig. 3. Identification of reactive gliosis in Müller cells via glial fibrillary acidic protein (GFAP) immunohistochemistry of the myopic retina. (**a**) GFAP expression increased in Müller cells of the myopic retina compared to that of control retina. (**b**) Quantitative analysis showed a significant increase in mean GFAP immunofluorescence intensity in the retina of myopic rabbits compared to controls.

presence of reactive gliosis in Müller cells, with notably increased GFAP expression[13,14], extending from the ganglion cell layer to the outer plexiform layer in myopic eyes, but not in those of the control rabbits. Myopic eyes also demonstrated a higher density of Müller cells, reflecting enhanced reactive gliosis (Fig. 3).

Validation of CD29+ cell identity in myopic rabbit retina

We conducted a detailed analysis to confirm that the CD29+ cells isolated via magnetically activated cell sorting (MACS) were Müller cells. While CD29 serves as an indicative marker of this population, it may not be sufficiently specific to conclusively identify Müller cells owing to the broad expression of CD29 in various cell types. To address this uncertainty, we performed immunostaining for the well-established Müller cell markers GFAP and glutamine synthetase (GLUL)[13–15]. Morphological examinations under an optical microscope revealed that CD29+ cells exhibited a larger and more elongated morphology, characteristic of Müller cells within the retinal layers. Cytoplasmic staining further confirmed strong CD29 expression in these cells as compared to the minimal expression in CD29- cells (Fig. 4a and b).

Further validation was achieved through immunofluorescence staining, wherein both GFAP and GLUL were prominently expressed within the cytoplasm of CD29+ cells, isolated from the central and peripheral regions of myopia-induced retina. This confirmed their identity as Müller cells (Fig. 4c). These findings indicate that the
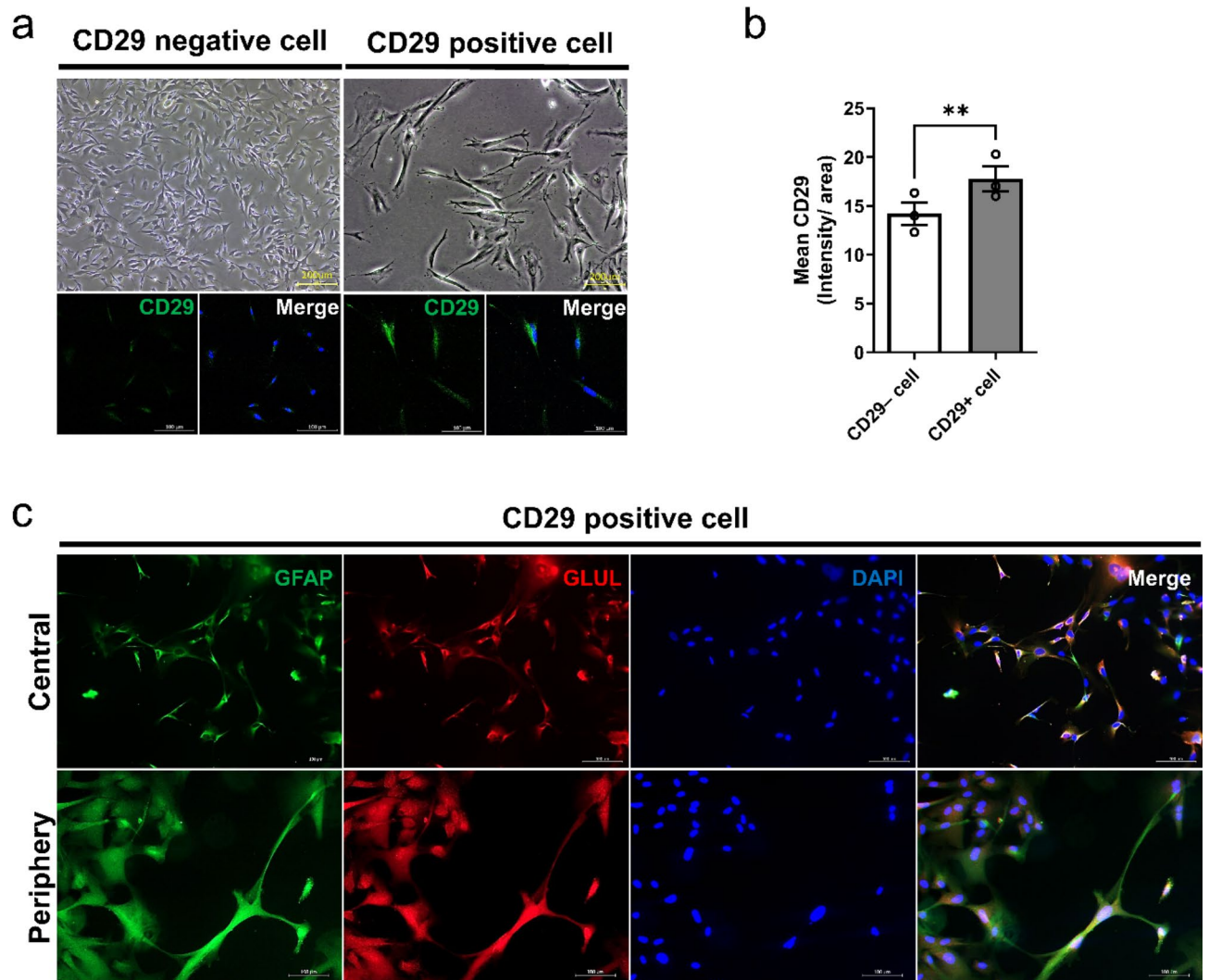
Fig. 4. Validation of CD29+ cell identity as Müller cells. (**a**) Comparison of CD29+ and CD29- cells revealed that CD29+ cells exhibited larger and more elongated morphology, characteristic of Müller cells, as opposed to CD29- cells. The cytoplasm of CD29+ cells showed a significantly stronger CD29 immunofluorescence signal, indicating effective isolation. (**b**) Quantitative analysis showed a significant increase in mean CD29 immunofluorescence intensity in the retina of myopic rabbits compared to controls. (**c**) Immunofluorescence staining of CD29+ cells from both the central and peripheral retinal regions demonstrated co-expression of glial fibrillary acidic protein (GFAP) and glutamine synthetase (GLUL), confirming their identity as Müller cells.

CD29+ cells isolated from myopic rabbit retina were indeed Müller cells, corroborating the specific morphology and expression typical of this cell type within the retina.

Proteomic analysis of CD29-positive Müller cells from the central and peripheral regions of the retina

To investigate protein alterations in pathological Müller cells within both the central and peripheral regions of the retina, we conducted a comprehensive proteomic analysis using CD29+ Müller cells derived from myopic rabbits. In total, 36 proteins were identified from the entire retina, including both the central and peripheral regions (Supplementary Table S1). A heat map of protein expression profiles revealed a distinct clustering of Müller-like cells between the myopia and control groups, highlighting significant differences in protein expression patterns (Fig. 5a). Despite these differences, the protein levels within the central and the peripheral regions were notably similar between groups.

The heat map also indicated an overall increase in protein expression in the myopia group compared to that in the control group. Gene Ontology (GO) biological process analysis indicated the involvement of these proteins in three specific signaling pathways:glycolysis involving glyceraldehyde-3-phosphate dehydrogenase (GAPDH), beta-enolase (ENO3), and fructose-bisphosphate aldolase A (ALDOA); positive regulation of sprouting angiogenesis associated with pyruvate kinase (PKM) and annexin A (ANXA1); and L-lactate dehydrogenase
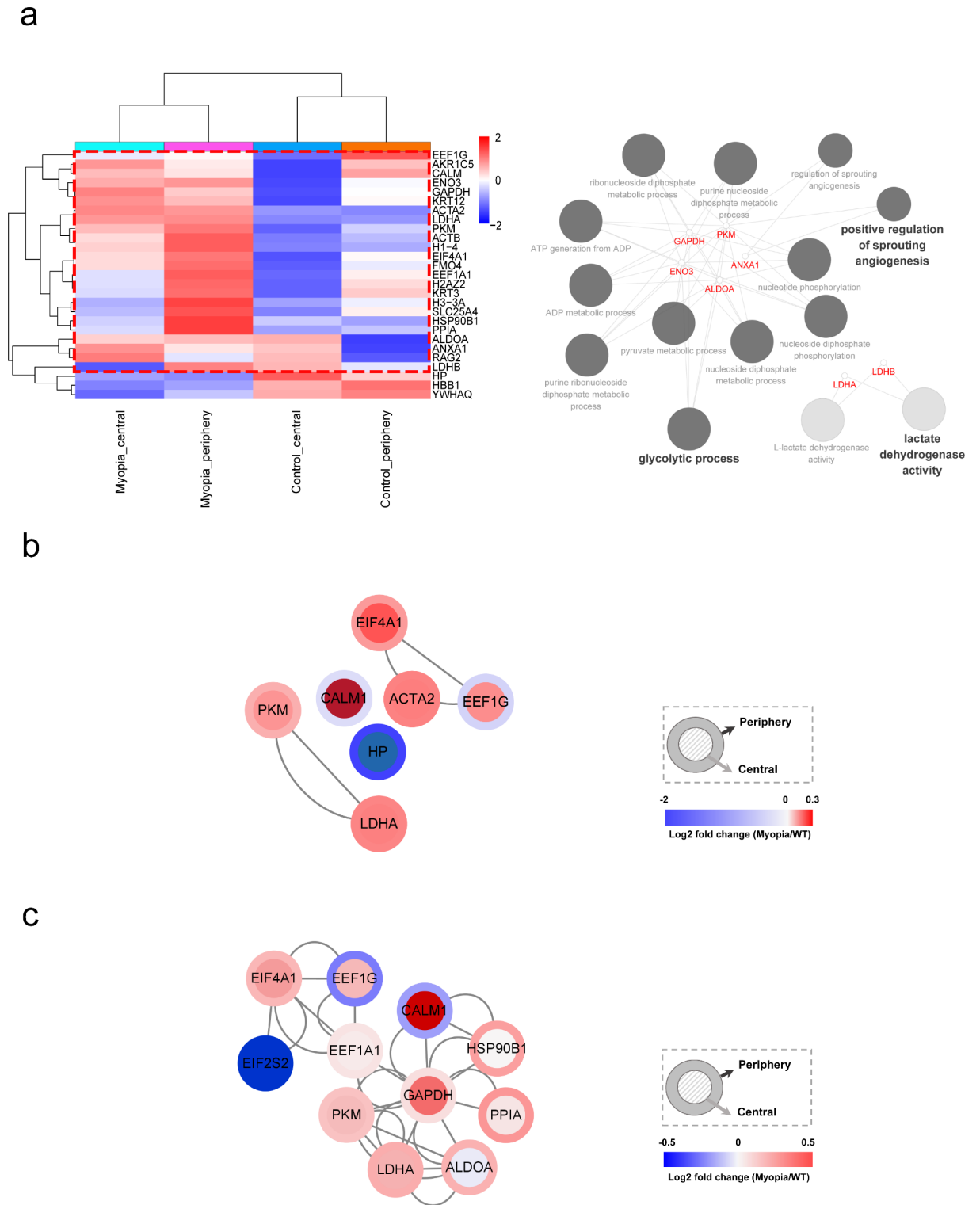
Fig. 5. Proteomics analysis of CD29+ Müller cells in the myopic retina of rabbits. (**a**) Heatmap depicting unsupervised hierarchical clustering of protein expression profiles in CD29+ Müller cells, highlighting significant differences between the myopic and control groups. The analysis includes a Gene Ontology biological process breakdown using ClueGO to identify key signaling pathways. (**b**) Protein-protein interaction (PPI) network constructed using differentially expressed proteins (p-value < 0.5), illustrating the interactions and potential regulatory mechanisms differentially regulated in the myopic retina. (**c**) Comprehensive protein-protein interaction (PPI) network incorporating proteins universally expressed in CD29+ Müller cells across both the central and peripheral regions of the retina.

A chain (LDHA) and L-lactate dehydrogenase B chain (LDHB) associated with lactate dehydrogenase activity (Fig. 5a).

Despite the identification of differentially expressed proteins (DEPs) with fold changes > 1.2 and p-value < 0.1 (Table 1), the number of DEPs was insufficient for a robust protein-protein interaction (PPI) analysis. In the central retina, proteins such as calmodulin (CALM) and keratin 12 (KRT12) were upregulated under myopia, whereas haptoglobin (HP), hemoglobin subunit beta 1 (HBB1), and eukaryotic translation initiation factor 2 subunit 2 (EIF2S2) were downregulated. In the peripheral retina, V(D)J recombination-activating protein 2 (RAG2) was upregulated, whereas HBB1 was downregulated.

To further explore the potential biological significance of these changes, we conducted a targeted PPI analysis of the seven DEPs that were commonly expressed in both the central and peripheral regions of the retina with p-values < 0.5 (Fig. 5b). This analysis identified specific interaction patterns, predominantly among proteins associated with metabolic processes. Notably, LDHA and PKM, both involved in glycolysis, were consistently upregulated in both the central and peripheral regions, which suggested adaptation to metabolic demands. Alpha-smooth muscle actin (ACTA2) also exhibited upregulation, consistent with the changes in cellular structure and contractility associated with myopic alterations. Conversely, HP expression decreased across both regions, indicating a potential shift in the protein stabilization and heme-scavenging pathways. Interestingly, CALM1 and elongation factor 1-gamma (EEF1G) showed regional differences in expression, increasing in the central while decreasing in the peripheral regions. These variations may reflect differential regional responses to myopic stress within the retina.

Owing to the limited number of DEPs, we extended the PPI analysis to include all proteins commonly expressed in CD29-positive Müller cells across the central and peripheral regions (Fig. 5c). This analysis highlighted eight upregulated proteins, namely, PKM, LDHA, GAPDH, EIF4A1, elongation factor 1-alpha 1 (EEF1A1), peptidyl-prolyl cis-trans isomerase A (PPIA), endoplasmin (HSP90B1), and ALDOA, as key components of an altered metabolic system in myopia, particularly affecting glycolytic processes. Conversely, EIF2S2, involved in cytoplasmic translation initiation, was commonly downregulated. Interestingly, CALM1 and EEF1G exhibited opposite regional expression trends, with increased expression in the central region and decreased expression in the peripheral region of the retina. When analyzing PPIs within each region separately, the patterns were consistent with those observed in the comprehensive analysis across regions (Fig. 5c and Supplementary Fig. S2).

We attempted to validate the increased expression of PKM and LDHA identified in our proteomic analysis through qRT-PCR. Due to insufficient quantities of isolated Müller cells, direct validation with these specific cells was not possible. Instead, we utilized whole retinal tissues from both the central and peripheral regions for this purpose. Notably, although the proteomic data indicated an upregulation of LDHA and PKM protein levels in the myopia group, our qRT-PCR results revealed a general decrease in the mRNA levels of these genes in comparison to the control group (Supplementary Fig. S3).

Discussion

Previous research has extensively explored the roles of oxidative stress and inflammatory processes in the development of myopia, particularly within the sclera and the broader retinal environment[16,17]. However, the specific contributions of Müller cells in these processes, particularly in the context of myopia, have been relatively underexplored. These cells are vital for retinal homeostasis and play integral roles in ion regulation, neurotransmitter recycling, and maintaining the blood-retinal barrier[18]. Recognizing this oversight, our study specifically targets the metabolic and proteomic shifts in Müller cells under myopic stress, a relatively underexplored area in myopic research.

This research extends beyond the structural examination to a molecular level, by examining the proteomic landscape within Müller cells derived from myopic rabbits. The observed increase in GFAP expression in Müller cells confirms reactive gliosis in response to myopia induction, highlighting significant adaptive changes in the retinal structure. By utilizing a MACS-based technique to isolate CD29+ Müller cells, followed by rigorous validation of these cells through immunostaining for GFAP and GLUL, we identified substantial alterations in glycolytic and angiogenic pathways. These findings suggest that the active response of Müller cells to the

Protein	Fold change	p-value
Central		
CALM	1.63	0.01
KRT12	1.37	0.02
HP	0.2	0.09
HBB1	0.06	0.07
EIF2S2	0.06	0.08
Periphery		
RAG2	1.22	0.08
HBB1	0.04	0.08

Table 1. Differential expressed proteins in CD29+ Müller cells from myopia-induced central and peripheral retina (fold change > 1.2, p-value < 0.1).

stress induced by myopia, marking a significant advancement in understanding their role in the development of myopia. Our approach fills a critical gap by elucidating the adaptive metabolic processes within Müller cells.

Recent studies using mouse and marmoset models of form deprivation-induced myopia have demonstrated increased GFAP expression in the retina, corroborating our findings in the rabbit model of myopia[19]. Another study showed that myopia induction leads to an increase in the number of GFAP-positive glial cells and a reduction in peripheral capillary branching, further supporting the structural reorganization of retinal astrocytes and the vascular framework during myopic alterations[20]. These consistent findings across different models highlight the common alterations in Müller cells within the retina following myopia induction.

Our findings demonstrated significant differences in the expression of glycolysis-related proteins in Müller cells from the central retina of myopic rabbits compared to controls. Specifically, the upregulation of key glycolytic enzymes, including GAPDH, ENO3, and ALDOA, suggests that Müller cells in the myopic retina increasingly rely on anaerobic glycolysis to meet heightened energy demands under oxygen-limited conditions[21–23]. This metabolic shift is further supported by the marked increase in LDHA expression, a hypoxia-inducible enzyme that converts pyruvate to lactate, indicating an adaptive response to the structural and functional challenges posed by myopia. In contrast, LDHB, which typically reconverts lactate to pyruvate and is less active under hypoxic conditions, showed minimal changes, highlighting a shift toward enhanced lactate production[24–26]. This pattern mirrors similar glycolytic adaptations seen in other retinal diseases like diabetic retinopathy, where hypoxia drives increased LDHA activity[27]. Moreover, our findings align with previous research by Yu et al., which also reported upregulation of LDHA in myopic retina, further validating the role of glycolysis in the retinal response to myopia[28]. The observed increase in glycolytic activity in Müller cells, along with elevated lactate levels, parallels the metabolic changes in the sclera during myopia-induced axial elongation and tissue remodeling. These results emphasize the critical role of enhanced glycolysis in Müller cells during myopia progression. However, our findings strongly indicate that glycolytic reprogramming plays a crucial role in the adaptation of Müller cells to myopic stress.

Additionally, the observed enhancement in sprouting angiogenesis suggests an adaptive response to the hypoxic environment within the myopic retina, as evidenced by the upregulation of PKM and ANXA1 in the PPI network (Fig. 5a). PKM plays a critical role in glycolysis, which is the primary ATP generation pathway for endothelial cells, and is essential for proper vascular function, including the internalization and trafficking of vascular endothelial cadherin at cell junctions[29]. Inhibition of PKM has been shown to suppress angiogenesis by reducing ATP production required for these processes[29]. Similarly, ANXA1, which is induced by hypoxic stimuli in the retina, plays a dual role in modulating both angiogenesis and inflammatory responses. While ANXA1 inhibits pro-inflammatory cytokines, it promotes reparative angiogenesis, providing a neuroprotective effect, particularly in conditions such as ischemic retinopathy[30]. This upregulation of PKM and ANXA1 suggests that Müller cells may contribute to vascular remodeling and help the retina adapt to the metabolic and structural stresses imposed by myopia.

Proteomic analysis of the central region of the retina revealed five DEPs between the myopic and control eyes—CALM, KRT12, HP, HBB1, and EIF2S2 (Table 1). CALM exhibited the most pronounced changes, which suggested a potential shift in calcium signaling[31]. Studies of lung epithelial cells exposed to nanoparticles have demonstrated that inhibition of CALM expression leads to increased ROS (Reactive oxygen species) production, indicating its involvement in mechanisms that manage or respond to oxidative stress in cells[32]. Such a role of CALM highlights its potential as a therapeutic target, whereby the modulation of calcium signaling could mitigate myopia progression.

Conversely, the downregulation of HP and HBB1 in Müller cells from myopic retina points to potential deficiencies in the management of ROS, leading to increased oxidative stress. When expressed in non-erythrocyte cells, hemoglobin detoxifies highly oxidizing radicals and alleviates the H_2O_2-induced oxidative stress[33,34]. Therefore, a reduction in HBB1 expression may lead to elevated levels of ROS, causing cellular damage and promoting the development of myopia. Previous studies have demonstrated the role of hemoglobin in scavenging ROS under oxidative stress, suggesting that decreased HBB1 expression could impair ROS management, thereby exacerbating tissue damage and contributing to the progression of myopia[35]. Similarly, HP binds free hemoglobin to prevent the iron within hemoglobin from catalyzing the formation of harmful free radicals that cause oxidative damage to cells[36]. Knock-out studies in mice have shown that the absence of HP makes them more prone to oxidative damage, indicating that a decrease in HP expression might also contribute to the tissue damage caused by myopia progression[37]. This intricate relationship among hypoxia, oxidative stress, and cellular damage in the myopic retina highlights the need for targeted interventions that address these metabolic and oxidative imbalances to potentially slow down or prevent further deterioration in myopia.

The current study has certain limitations. First, although the MACS-based Müller cell isolation method effectively yielded CD29+ Müller cells, the potential inclusion of other neuronal and glial cells in the sample cannot be entirely ruled out. However, the strong expression of Müller cell markers such as GFAP and GLUL in the isolated cells supports their identification[38]. Second, the limited availability of isolated Müller cells restricted not only our ability to perform RNA-seq but also limited the scope of direct quantitative validation experiments. Ideally, RNA-seq would precede proteomic analysis to provide a comprehensive molecular profile; however, due to insufficient cell quantities, this step could not be executed. In addition, to validate the protein expression changes observed in our proteomic analysis, we employed qRT-PCR using whole retinal tissues instead of isolated Müller cells. This adaptation was necessary but introduced discrepancies between mRNA and protein expression levels, possibly indicating post-transcriptional modifications or regulatory mechanisms that could not be directly assessed within the Müller cells. Future studies with adequate cell quantities are essential to enable both comprehensive RNA and protein analyses directly on Müller cells to clarify these mechanisms. Third, while proteomics data reveal which proteins are differentially expressed, they do not establish the actual signaling pathway that is activated or suppressed in myopic retina. Additional research is needed to map such

pathways, particularly those related to oxidative stress, through the use of pathway inhibitors or activators in a controlled setting to confirm the implications of observed protein expression changes.

In conclusion, our study offers novel insights into the metabolic reprogramming of Müller cells in response to the tissue remodeling that occurs during myopia. The significant upregulation of glycolytic and angiogenic pathways underscores the active role Müller cells play in adapting to the metabolic stress induced by myopia. These findings enhance our understanding of the cellular mechanisms driving myopia progression and provide a foundation for future research that can further explore the therapeutic potential of targeting these metabolic pathways to mitigate myopia progression.

Methods

Animals

Four 5–6-week-old New Zealand rabbits, weighing 1.5–2 kg, were obtained from the Department of Laboratory Animal Resources, Yonsei Biomedical Research Institute, Yonsei University College of Medicine. All animals were raised in accordance with the guidelines specified by the Institutional Animal Care and Use Committee, at a temperature of 25 °C and a 12-h light-dark cycle. The animal study protocol was approved by the Institutional Ethics Committee of the Department of Laboratory Animal Resources, Yonsei Biomedical Research Institute, Yonsei University College of Medicine (approval no. 2021-0054). This study was carried out in strict accordance with the recommendations in the ARRIVE guidelines. All surgery was performed under anesthesia, and every effort was made to minimize suffering.

Form deprivation myopia induction

We used the same method for form deprivation myopia induction as in our previous study[7]. Anesthesia was induced through subcutaneous injection of Zoletil (0.3 mL/kg, Virbac, Carros, France) and Rompun (0.2 mL/kg, Elanco, Indiana, US). To manage local pain and minimize bleeding, additional subcutaneous injections of Xylocaine (lidocaine HCl 2%: epinephrine mix = 1:100,000, Yuhan, Seoul, Korea) were administered above and below the eye. A horizontal incision was then made on the right eyelid to form two layers—inner and outer. The left eye was left untreated to serve as a control, while the right eye underwent light deprivation to induce myopia for comparison of the experimental effects. The inner layer was sutured with 6‑0 Vicryl (Ethicon, Raritan, NJ, USA) and the outer layer with 5‑0 Nylon (Ethicon, Raritan, NJ, USA). Postoperatively, Baytril (0.1 mL/kg, Elanco, Indiana, USA) and Keromin (0.1 ml, Hana Pharm, Hwaseong-si, Korea) were injected for 7 days to manage pain and prevent inflammation. Additionally, Tarivid (Santen, Osaka, Japan) was applied topically to the surgical site during this period for the same purposes. The Nylon sutures in the outer layer were removed after 7 days. The sutured eyelids were maintained for 4 weeks. Thereafter, the same anesthesia protocol was followed, and the eyelid surgery site was incised to examine the eyeball. Axial length measurements were conducted using an A-scan ultrasound (UD-6000, Tomey, Nagoya, Japan). After local anesthesia of the eye with proparacaine (Hanmi, Seoul, Republic of Korea), measurements were taken by placing the device in contact with the cornea. Once the alignment was accurately set from the cornea to the retina, more than seven measurements were taken, and the average value was calculated. The refractive error was measured using streak retinoscopy both before and after myopia induction.

Retinal tissue preparation

In this study, rabbits were initially anesthetized using Zoletil (0.3 mL/kg, Virbac, Carros, France) and Rompun (0.2 mL/kg, Bayer Animal Health, Germany) administered intramuscularly to ensure adequate sedation for the procedures. After confirming deep anesthesia by verifying the absence of reflexes, potassium chloride (KCl) at a dosage of 1 mL/kg was administered intravenously to induce cardiac arrest. The use of KCl under anesthesia ensured that the animals experienced a humane and painless death. This method adhered to institutional ethical guidelines and followed the AVMA Guidelines for the Euthanasia of Animals. After euthanasia, the eyeballs were promptly enucleated. The eyeballs from one rabbit were designated as whole-retinal block preparations for immunofluorescence staining. The remaining three pairs of eyeballs were used for retinal tissue preparation. The cornea, lens, and vitreous humor were excised, and the remaining eyeball was cut into a petaloid configuration. The retina was segmented into central and peripheral regions based on the distance from the visual streak to the limbus. Each region was separately immersed in Dulbecco's phosphate-buffered saline (DPBS; Thermo Fisher Scientific, Waltham, MA, USA).

Isolation of Müller cells from rabbit retina

Following segmentation, the retinal tissue was enzymatically dissociated into single cells using the Neural Tissue Dissociation Kit – Postnatal Neurons (Miltenyi Biotec, Bergisch Gladbach, German), as described in a prior study[39]. To eliminate microglia and vascular endothelial cells, the cell suspension was treated with CD11b-FITC (6 µg/ml, MA110081, Invitrogen, Waltham, MA, USA) and CD31-FITC (4 µg/ml, NBP2-33136 F, Novus Biologicals, Minneapolis, MN, USA) antibodies at 4 °C for 30 min. Subsequent separation involved the application of Anti-FITC Microbeads (Miltenyi Biotec, Bergisch Gladbach, Germany) for 15 min at 4 °C, followed by magnetic sorting using an MS column. For selective enrichment of Müller cells, CD29-FITC (1:50, bs-0486R-FITC, Bioss, Woburn, MA, USA) was added and incubated at 4 °C for another 30 min. The cells were then washed with DPBS, mixed with microbeads, and again passed through an MS column to segregate the CD29+ and CD29- cell populations.

Protein extraction and processing

Proteins were extracted from Müller cells obtained from three distinct retinal samples. Each sample was lysed in 8 M Urea and 100 mM ammonium bicarbonate, followed by sonication. The lysate was centrifuged at 14,000 rpm

for 15 min to collect the supernatant containing proteins. Protein concentration was quantified using a micro BCA protein assay according to the manufacturer's instructions (23235, Thermo Fisher Scientific, Waltham, MA, USA). The Seppro IgY Depletion Kit (Sigma-Aldrich, St Louis, MO, USA) was used to eliminate antibodies and reduce protein abundance. Protein denaturation and reduction were achieved by adding 10 mM DTT, and alkylation was performed using 30 mM iodoacetamide (IAA). Digestion was performed overnight at 37 °C with trypsin and stopped by adding 0.4% trifluoroacetic acid. The peptides were purified using a Pierce C18 Spin Column, dried, and stored at -80 °C until further analysis.

Protein identification using LC-MS/MS

For Label-Free Quantification (LFQ) analysis, peptides were reconstituted in 0.1% formic acid (FA) in water and analyzed using a Q Exactive HF-X mass spectrometer (Thermo Fisher Scientific, Waltham, MA, USA) coupled to a nano EASY-nLC 1000 system (Thermo Fisher Scientific, Seattle, WA, USA). The peptides (2 μg) were loaded onto a trap column (acclaim PepMap 100, 75 μm × 2 cm, 3 μm, C18, 100 Å) in buffer A (0.1% formic acid) and ionized via a spray column (PepMap RSLC C18, 50 cm × 75 μm ID) packed with 2 μm C18 particles at an electric potential of 1.8 kV. Peptides were eluted using a gradient of buffer B (0.1% FA in acetonitrile) ranging from 5 to 80% at a flow rate of 300 nL/min. Full MS data were acquired in a scan range of 400–2000 Th at a resolution of 60,000. The automated gain control (AGC) target value was set at 3.0×10^6, with a maximum ion injection time of 100 ms for the MS scans. The top 20 most abundant ions with an isolation window of 2.0 m/z were fragmented via data-dependent MS/MS experiments with an exclusion duration of 30 s and a normalized collision energy of 27 for HCD. The maximum ion injection time for MS/MS scans was 100 ms, and the AGC target value was set at 1.0×10^6.

Raw data processing and proteomics data analysis

For data analysis profiling, the MS/MS spectra were searched using the proteome discoverer software version 2.5 (Thermo Fisher Scientific, Waltham, MA, USA) against the UniProt rabbit proteome database, which was last updated in November 2023. The criteria for protein identification included the detection of at least one unique peptide per protein. Specific attention was paid to unique peptides that were altered by carbamidomethylation of cysteine residues, N-acetylation, or methionine oxidation. To maintain rigorous quality control, a false discovery rate cutoff of 1% was used at both the peptide spectrum match and protein levels. Log2 transformation was applied to all LFQ intensities to minimize the impact of outliers, and sum normalization was used to correct for biological and technical variations in the dataset. Missing protein values in any group were excluded to enhance data reliability.

Protein intensities were normalized by total sum scaling to make them comparable, and the ratio of the mean value of normalized protein intensities was calculated for each protein. Statistical and bioinformatics evaluation of the proteomics data, utilizing normalized protein abundance, was conducted using R (version 4.4.0, as of May 2024). This included clustering analyses such as heatmap and hierarchical clustering, which employed Euclidean distances and Ward's linkage methods to elucidate the variances and distinctions between the samples. Differential expression was determined based on proteins exhibiting at least a 1.2-fold change in LFQ intensity and a p-value < 0.1, as calculated via Student's t-test. However, the number of DEPs identified using these criteria was too small to perform a robust Gene Ontology (GO) analysis (Table 1).

GO enrichment and network analyses

To address this limitation, we expanded our analysis to include all the identified proteins, categorizing them based on whether they showed an increase or decrease in fold change under the myopic condition compared to that under the control conditions, regardless of their p-values. This approach allowed for a more inclusive analysis of proteomic shifts between conditions and facilitated the comprehensive exploration of GO annotation and network interactions.

GO biological processes associated with the identified proteins and DEPs were examined using the Database for Annotation, Visualization, and Integrated Discovery, along with the g: Profiler online tool[40]. Protein networks and interactomes relating to the DEPs were explored using the public database STRING 12.0 and were visualized using Cytoscape. Furthermore, the ClueGO plugin for Cytoscape (version 2.5.10, available at https://apps.cytoscape.org/apps/cluego, accessed March 2024) was employed to organize and visualize GO terms, drawing on UniProt GO annotations for this analysis.

Confirmation of reactive gliosis via immunofluorescence staining

To confirm the presence of reactive gliosis in the retina following myopia induction, GFAP expression was assessed using immunofluorescence staining. The whole eyeball was fixed in 4% paraformaldehyde for 3 days, embedded in paraffin, and sectioned into 4 μm-slides. Slides were deparaffinized using xylene and rehydrated using a graded series of ethanol. Antigen retrieval involved heating the sections at 95 °C for 30 min in citrate buffer for antigen retrieval. Sections were blocked at room temperature for 1 h using 10% normal goat serum (50062Z, Thermo Fisher Scientific, Waltham, MA, USA) to prevent nonspecific antibody binding. Subsequently, the slides were incubated overnight at 4 °C with an anti-GFAP antibody (ab7260, Abcam, Cambridge, UK). After incubation with the primary antibody, the slides were washed several times with PBS to remove any unbound antibodies and then incubated with the anti rabbit alexa fluor 647 antibody (711-605-152, Jackson ImmunoResearch, West Grove, PA, USA) at room temperature for 1 h. Nuclei were stained with DAPI during the final wash step for 5 min. After staining, the slides were washed with PBS to remove excess DAPI and residual antibodies. The prepared slides were mounted using anti-fade mounting medium and covered with coverslips. Immunofluorescence images of the stained sections were captured using an Axio Imager M2 microscope (Carl

Zeiss, Oberkochen, Land Baden-Württemberg, Germany) and analyzed using the Zen software (Carl Zeiss, Oberkochen, Land Baden-Württemberg, Germany).

Immunofluorescence staining of the isolated CD29+ cells

CD29+ cell fractions were plated onto 4-well chamber slides to facilitate cell adherence. Once the cells had adhered, the slides were gently washed with PBS and fixed with 4% paraformaldehyde (PFA; Biosesang, Yongin, Korea) at room temperature. For permeabilization, 0.1% Triton X-100 in PBS was added to the samples. To block nonspecific binding, the cells were incubated with 10% normal goat serum (50062Z, Thermo Fisher Scientific, Waltham, MA, USA) at room temperature for 1 h. Overnight incubation at 4 °C was carried out with primary antibodies against GLUL (ab73593, Abcam, Cambridge, UK) and GFAP (G3893, Sigma Aldrich, St Louis, MO, USA), which were specifically selected to verify the identity of Müller cells[38,41]. Following incubation with primary antibodies, the slides were washed and then incubated with the anti rabbit alexa fluor 647 (711-605-152, Jackson ImmunoResearch, West Grove, PA, USA) and anti mouse alexa fluor 488 (A11001, Invitrogen, Waltham, MA, USA) at room temperature for an additional hour. Nuclei were stained with DAPI. Immunofluorescence images were captured using an Axio Imager M2 microscope (Carl Zeiss Oberkochen, Land Baden-Württemberg, Germany). Fluorescence intensity was quantified using ImageJ software (National Institutes of Health, Bethesda, MD, USA). Following the acquisition of fluorescence images, regions of interest (ROIs) were manually selected for each sample. The mean fluorescence intensity within each ROI was measured, and background fluorescence was subtracted to correct for non-specific signal. The quantified fluorescence intensities were averaged across multiple independent samples to ensure the reliability and reproducibility of the results.

Validation of selected Müller cell enriched genes using qRT-PCR

Due to limited quantity of isolated Müller cells, direct validation using these cells was not feasible. As an alternative approach, we utilized whole retinal tissues from the central and peripheral regions to validate our findings. qRT-PCR was performed for LDHA and PKM, which were consistently upregulated in both regions according to our proteomic analysis. Whole RNA was extracted from the central and peripheral regions of the rabbit retina using Trizol reagent (15596026, Invitrogen, Waltham, MA, USA). The extracted RNA was synthesized into cDNA using a premix. RT-qPCR reactions were performed on a QuantStudio 3 system (Applied Biosystems, Waltham, MA, USA) using Power SYBR™ Green PCR Master Mix (4367659, Applied Biosystems™, Waltham, MA, USA). The relative expression of the target genes was calculated using the comparative threshold method, normalized to the GAPDH housekeeping gene. The primer sequences are listed in Supplementary Table S2.

Data availability

Data are available via ProteomeXchange with the identifier PXD053804.

References

1. Holden, B. A. et al. Global prevalence of myopia and high myopia and temporal trends from 2000 through 2050. *Ophthalmology.* **123**, 1036–1042. https://doi.org/10.1016/j.ophtha.2016.01.006 (2016).
2. Frick, K. D. What the comprehensive economics of blindness and visual impairment can help us understand. *Indian J. Ophthalmol.* **60**, 406–410. https://doi.org/10.4103/0301-4738.100535 (2012).
3. Holden, B. et al. Myopia, an underrated global challenge to vision: Where the current data takes us on myopia control. *Eye (London England).* **28**, 142–146. https://doi.org/10.1038/eye.2013.256 (2014).
4. Mérida, S. et al. Glutathione and a pool of metabolites partly related to oxidative stress are associated with low and high myopia in an altered bioenergetic environment. *Antioxid. (Basel Switzerland).* **13**. https://doi.org/10.3390/antiox13050539 (2024).
5. Yu, Q. et al. Association between inflammatory cytokines and oxidative stress levels in aqueous humor with axial length in human myopia. *Exp. Eye Res.* **237**, 109670. https://doi.org/10.1016/j.exer.2023.109670 (2023).
6. Wu, W. et al. Hypoxia-induced scleral HIF-2α upregulation contributes to rises in MMP-2 expression and myopia development in mice. *Invest. Ophthalmol. Vis. Sci.* **63** https://doi.org/10.1167/iovs.63.8.2 (2022). 2.
7. Moon, C. E. et al. Retinal proteome analysis reveals a region-specific change in the rabbit myopia model. *Int. J. Mol. Sci.* **24** https://doi.org/10.3390/ijms24021286 (2023).
8. Reichenbach, A. & Bringmann, A. Glia of the human retina. *Glia.* **68**, 768–796. https://doi.org/10.1002/glia.23727 (2020).
9. Wang, D., Gao, F., Hu, F. & Wu, J. Nobiletin alleviates astrocyte activation and oxidative stress induced by hypoxia in vitro. *Molecules (Basel Switzerland).* **27**. https://doi.org/10.3390/molecules27061962 (2022).
10. Ding, X. et al. Inhibition of NF-κB ameliorates aberrant retinal glia activation and inflammatory responses in streptozotocin-induced diabetic rats. *Ann. Transl. Med.* **11**, 197. https://doi.org/10.21037/atm-22-2204 (2023).
11. Lee, S. H., Park, Y. S., Paik, S. S. & Kim, I. B. Differential Response of Müller Cells and Microglia in a mouse retinal detachment model and its implications in detached and non-detached regions. *Cells.* **10** https://doi.org/10.3390/cells10081972 (2021).
12. Wu, L. H. et al. A novel HDAC8 inhibitor H7E exerts retinoprotective effects against glaucomatous injury via ameliorating aberrant Müller glia activation and oxidative stress. *Biomed. Pharmacother.* **174**, 116538. https://doi.org/10.1016/j.biopha.2024.116538 (2024).
13. Lewis, G. P. & Fisher, S. K. Up-regulation of glial fibrillary acidic protein in response to retinal injury: Its potential role in glial remodeling and a comparison to vimentin expression. *Int. Rev. Cytol.* **230**, 263–290. https://doi.org/10.1016/s0074-7696(03)30005-1 (2003).
14. Inman, D. M. & Horner, P. J. Reactive nonproliferative gliosis predominates in a chronic mouse model of glaucoma. *Glia.* **55**, 942–953. https://doi.org/10.1002/glia.20516 (2007).
15. Hollborn, M. et al. The human Müller cell line MIO-M1 expresses opsins. *Mol. Vis.* **17**, 2738–2750 (2011).
16. McBrien, N. A. & Gentle, A. Role of the sclera in the development and pathological complications of myopia. *Prog. Retin. Eye Res.* **22**, 307–338. https://doi.org/10.1016/s1350-9462(02)00063-0 (2003).
17. Norton, T. T. & Siegwart, J. T. Jr. Light levels, refractive development, and myopia–A speculative review. *Exp. Eye Res.* **114**, 48–57. https://doi.org/10.1016/j.exer.2013.05.004 (2013).

18. Bringmann, A. et al. Müller cells in the healthy and diseased retina. *Prog. Retin. Eye Res.* **25**, 397–424. https://doi.org/10.1016/j.preteyeres.2006.05.003 (2006).
19. Zhang, X. et al. Functions of retinal astrocytes and Müller cells in mammalian myopia. *BMC Ophthalmol.* **22**, 451. https://doi.org/10.1186/s12886-022-02643-0 (2022).
20. Lin, C. et al. Myopia alters the structural organization of the retinal vasculature, GFAP-positive glia, and ganglion cell layer thickness. *Int. J. Mol. Sci.* **23**. https://doi.org/10.3390/ijms23116202 (2022).
21. Hurley, J. B., Lindsay, K. J. & Du, J. Glucose, lactate, and shuttling of metabolites in vertebrate retinas. *J. Neurosci. Res.* **93**, 1079–1092. https://doi.org/10.1002/jnr.23583 (2015).
22. Hurley, J. B. & Chao, J. R. It's never too late to save a photoreceptor. *J. Clin. Invest.* **125**, 3424–3426. https://doi.org/10.1172/jci83194 (2015).
23. Winkler, B. S., Arnold, M. J., Brassell, M. A. & Puro, D. G. Energy metabolism in human retinal Müller cells. *Invest. Ophthalmol. Vis. Sci.* **41**, 3183–3190 (2000).
24. Han, J. Y. S. et al. Role of monocarboxylate transporters in regulating metabolic homeostasis in the outer retina: Insight gained from cell-specific Bsg deletion. *FASEB J.*. **34**, 5401–5419. https://doi.org/10.1096/fj.201902961R (2020).
25. Ždralević, M. et al. Double genetic disruption of lactate dehydrogenases a and B is required to ablate the Warburg effect restricting tumor growth to oxidative metabolism. *J. Biol. Chem.* **293**, 15947–15961. https://doi.org/10.1074/jbc.RA118.004180 (2018).
26. Buono, R. J. & Lang, R. K. Hypoxic repression of lactate dehydrogenase-B in retina. *Exp. Eye Res.* **69**, 685–693. https://doi.org/10.1006/exer.1999.0745 (1999).
27. Yeo, E. J. Hypoxia and aging. *Exp. Mol. Med.* **51**, 1–15. https://doi.org/10.1038/s12276-019-0233-3 (2019).
28. Yu, F. J. et al. Alteration of retinal metabolism and oxidative stress may implicate myopic eye growth: Evidence from discovery and targeted proteomics in an animal model. *J. Proteom.* **221**, 103684. https://doi.org/10.1016/j.jprot.2020.103684 (2020).
29. Gómez-Escudero, J. et al. PKM2 regulates endothelial cell junction dynamics and angiogenesis via ATP production. *Sci. Rep.* **9**, 15022. https://doi.org/10.1038/s41598-019-50866-x (2019).
30. Hui, Q., Zheng, F., Qin, L. & Pei, C. Annexin A1 promotes reparative angiogenesis and ameliorates neuronal injury in ischemic retinopathy. *Curr. Eye Res.* **47**, 791–801. https://doi.org/10.1080/02713683.2022.2029904 (2022).
31. Swulius, M. T. & Waxham, M. N. Ca(2+)/calmodulin-dependent protein kinases. *Cell. Mol. Life Sci.* **65**, 2637–2657. https://doi.org/10.1007/s00018-008-8086-2 (2008).
32. Verma, N., Pink, M. & Schmitz-Spanke, S. A new perspective on calmodulin-regulated calcium and ROS homeostasis upon carbon black nanoparticle exposure. *Arch. Toxicol.* **95**, 2007–2018. https://doi.org/10.1007/s00204-021-03032-0 (2021).
33. Nishi, H. et al. Hemoglobin is expressed by mesangial cells and reduces oxidant stress. *J. Am. Soc. Nephrol. JASN.* **19**, 1500–1508. https://doi.org/10.1681/asn.2007101085 (2008).
34. Liu, W., Baker, S. S., Baker, R. D., Nowak, N. J. & Zhu, L. Upregulation of hemoglobin expression by oxidative stress in hepatocytes and its implication in nonalcoholic steatohepatitis. *PloS One.* **6**, e24363. https://doi.org/10.1371/journal.pone.0024363 (2011).
35. Orrico, F. et al. Oxidative stress in healthy and pathological red blood cells. *Biomolecules*. **13**https://doi.org/10.3390/biom13081262 (2023).
36. Miller, Y. I., Altamentova, S. M. & Shaklai, N. Oxidation of low-density lipoprotein by hemoglobin stems from a heme-initiated globin radical: Antioxidant role of haptoglobin. *Biochemistry*. **36**, 12189–12198. https://doi.org/10.1021/bi970258a (1997).
37. Bertaggia, E. et al. Haptoglobin is required to prevent oxidative stress and muscle atrophy. *PloS One*. **9**, e100745. https://doi.org/10.1371/journal.pone.0100745 (2014).
38. Pekny, M. & Nilsson, M. Astrocyte activation and reactive gliosis. *Glia*. **50**, 427–434. https://doi.org/10.1002/glia.20207 (2005).
39. Kaplan, L. et al. Retinal regions shape human and murine Müller cell proteome profile and functionality. *Glia*. **71**, 391–414. https://doi.org/10.1002/glia.24283 (2023).
40. Huang da, W., Sherman, B. T. & Lempicki, R. A. Systematic and integrative analysis of large gene lists using DAVID bioinformatics resources. *Nat. Protoc.* **4**, 44–57. https://doi.org/10.1038/nprot.2008.211 (2009).
41. Bringmann, A. & Wiedemann, P. Müller glial cells in retinal disease. *Ophthalmologica*. **227**, 1–19. https://doi.org/10.1159/000328979 (2012).

Acknowledgements

Author contributions
C.E.M. and J.K.L. contributed conducting the experiments, data acquisition, data analysis, and manuscript writing. H.K., Y.K., and J.K. performed experiments. J.H. contributed to the study design and data analysis. Y.W.J. and Y.S. contributed to the study design, conducted experiments, acquired, and analyzed the data, and wrote the manuscript. All the authors have read and agreed to the published version of the manuscript.

Funding

Declarations

Competing interests
The authors declare no competing interests.

Additional information
Supplementary Information The online version contains supplementary material available at https://doi.org/10.1038/s41598-024-75637-1.

Correspondence and requests for materials should be addressed to Y.W.J. or Y.S.

Reprints and permissions information is available at www.nature.com/reprints.